HHS Public Access

Author manuscript

Science. Author manuscript; available in PMC 2015 November 15.

Published in final edited form as:

Science. 2015 May 15; 348(6236): 799–803. doi:10.1126/science.aaa5175.

Microtubule detyrosination guides chromosomes during mitosis

Marin Barisic[1,2], **Ricardo Silva e Sousa**[3,#], **Suvranta K. Tripathy**[3,#], **Maria M. Magiera**[4,5,6,#], **Anatoly V. Zaytsev**[3,7,8], **Ana L. Pereira**[1,2], **Carsten Janke**[4,5,6], **Ekaterina L. Grishchuk**[3,*,†], and **Helder Maiato**[1,2,9,*,†]

[1]Chromosome Instability & Dynamics Laboratory, Instituto de Biologia Molecular e Celular, Universidade do Porto, Rua do Campo Alegre 823, 4150-180 Porto, Portugal

[2]Instituto de Investigação e Inovação em Saúde – i3S, Universidade do Porto, Portugal

[3]Physiology Department, Perelman School of Medicine, University of Pennsylvania, Philadelphia, Pennsylvania, USA

[4]Institut Curie, 91405 Orsay, France

[5]PSL Research University, 75005 Paris, France

[6]Centre National de la Recherche Scientifique UMR 3348, 91405 Orsay, France

[7]Center for Theoretical Problems of Physicochemical Pharmacology, RAS, Moscow, Russia

[8]Federal Research and Clinical Centre of Pediatric Hematology, Oncology and Immunology, Moscow, Russia

[9]Cell Division Unit, Department of Experimental Biology, Faculdade de Medicina, Universidade do Porto, Alameda Prof. Hernâni Monteiro, 4200-319 Porto, Portugal

Abstract

Before chromosomes segregate into daughter cells they align at the mitotic spindle equator, a process known as chromosome congression. CENP-E/Kinesin-7 is a microtubule plus-end-directed kinetochore motor required for congression of pole-proximal chromosomes. Because the plus-ends of many astral microtubules in the spindle point to the cell cortex, it remains unknown how CENP-E guides pole-proximal chromosomes specifically towards the equator. Here we found that congression of pole-proximal chromosomes depended on specific post-translational detyrosination of spindle microtubules that point to the equator. In vitro reconstitution experiments demonstrated that CENP-E-dependent transport was strongly enhanced on detyrosinated microtubules. Blocking tubulin tyrosination in cells caused ubiquitous detyrosination of spindle microtubules and CENP-E transported chromosomes away from spindle poles in random

*Correspondence to: maiato@ibmc.up.pt or gekate@mail.med.upenn.edu.
#†Equal contributions

The authors declare no conflict of interests.

Supplementary Materials:
Materials and Methods
Figures S1–S12
Table S1
Movies S1–S5
References (*28–43*)

directions. Thus, CENP-E-driven chromosome congression is guided by microtubule detyrosination.

Chromosome congression is the process that leads to the formation of a metaphase plate at the equator of mitotic cells. During congression, peripheral chromosomes are first brought to the vicinity of spindle poles by the microtubule minus-end-directed kinetochore motor Dynein, and are subsequently transported towards the equator by the plus-end-directed kinetochore motor CENP-E/Kinesin-7 (1–3). Because different kinetochore motors are able to move chromosomes in opposite directions along anisotropic spindle microtubules, how chromosomes are guided towards the equator remains a critical longstanding question. This might involve spatial cues provided by intracellular gradients, such as the RanGTP gradient, which becomes established around aligned chromosomes (4). We tested this possibility by expressing the dominant-negative mutant RanT24N (5), which fails to bind GTP and inhibits RCC1-dependent RanGTP gradient formation from chromosomes, but found no major congression problems in human U2OS cells (Fig. S1). Alternatively, the activity and/or affinity of kinetochore motors to microtubules might itself be regulated (e.g. by phosphorylation) (6, 7). This model would account for the relative dominance of different kinetochore motors in time and space, but it fails to explain the biased motion of pole-proximal chromosomes towards the equator. A third hypothesis predicts that kinetochore motors are sensitive to spatial cues encoded by the microtubule tracks they move on, which determine the direction of chromosome motion. These spatial cues may result from different stability within spindle microtubules (e.g. astral vs. kinetochore microtubules), or from their different organization (e.g. individual vs. bundled microtubules). However, recent work has shown that stable kinetochore microtubule bundles are dispensable for CENP-E-mediated chromosome congression (8), suggesting a different mechanism.

One possibility is that tubulin post-translational modifications (PTMs) generate specific cues that guide CENP-E along specific spindle microtubules. This so-called “tubulin code” has been proposed to contribute to subcellular differentiation of microtubules (9, 10), and tubulin acetylation and detyrosination are specifically enriched on stable spindle microtubules that point to the equator (11–13). Tubulin acetylation and detyrosination were shown to regulate Kinesin-1-dependent transport in neurons (14–16), and recent in vitro reconstitution experiments have also demonstrated subtle, but direct effects of tubulin PTMs on the motor activities of Kinesin-2, Kinesin-13 and Dynein (17).

To test whether tubulin detyrosination and acetylation are required for chromosome congression, we perturbed the function of enzymes responsible for specific catalytic steps (Fig. S2A,B). To modulate tubulin detyrosination in human U2OS cells we overexpressed tubulin tyrosine ligase (TTL), which specifically converts soluble α-tubulin to its tyrosinated form (18). In parallel, we inhibited tubulin carboxypeptidase (TCP) with the cell-permeable drug parthenolide (19), thus preventing removal of the C-terminal tyrosine from polymerized α-tubulin (10). Both treatments specifically decreased tubulin detyrosination without affecting polyglutamylation (Fig. 1A, Fig. S3), and reduced the detyrosination of spindle microtubules pointing to the equator (Fig. 1B, Fig. S4A). These cells consistently showed misaligned pole-proximal chromosomes and delayed mitotic progression,

phenocopying CENP-E inhibition (Fig. 1B, Fig. S4B, Movie S1). In contrast, perturbation of tubulin acetylation had no effect on chromosome congression (Fig. S5A–C). Thus, detyrosination of spindle microtubules pointing to the equator is required for congression of pole-proximal chromosomes.

Whereas CENP-E is mostly associated with kinetochores during early mitosis, we noticed that CENP-E-GFP expressed under control of its own promoter (20) specifically co-localized with the few detyrosinated microtubules (D-MTs) present in HeLa cells in G2 (21) (Fig. S6A,B). Moreover, inhibition of tubulin detyrosination with parthenolide led to CENP-E dissociation from these microtubules (Fig. S7A,B, Fig. S4A, Movie S2), suggesting that tubulin detyrosination promotes the interaction between CENP-E and microtubules in vivo. To test whether this tubulin PTM affects CENP-E directly, we reconstituted CENP-E motility in vitro using purified components. Brain tubulin was not suitable for these experiments because it is highly detyrosinated and carries many other PTMs (Fig. 2A). We thus developed a method to purify tyrosinated tubulin from HeLa cells using cycles of polymerization and depolymerization (22). A fraction of this tubulin was then treated with carboxypeptidase A to produce detyrosinated tubulin (Fig. 2A). These purified proteins were used to polymerize D- and T-MTs, and motility of recombinant CENP-E-GFP was examined using total internal reflection fluorescence microscopy (Fig. S8A, Movie S3). CENP-E bound to and moved processively and unidirectionally on both types of microtubules, but it was faster on D- vs. T-MTs: 31.3±0.7 vs. 26.7±0.4 μm/min, respectively (Fig. 2B, Fig. S8B). Moreover, there was a ~60% increase in the characteristic length of CENP-E runs on D- vs. T-MTs (1.55±0.06 vs. 0.97±0.07 μm), implying that CENP-E walks more processively on D-MTs assembled in vitro.

We next investigated the force produced by single CENP-E motors using a stationary optical trap (23). CENP-E motors carrying a C-terminal 6xHis-tag were linked to 0.54-μm streptavidin-coated polystyrene beads with biotinylated anti-His antibodies. The beads were then positioned near the microtubule using an infrared laser and their motility was examined in a buffer with physiological levels of ATP. Bead-microtubule binding frequencies were similar for these two types of microtubules (0.41 and 0.45 s^{-1} for D- and T-MTs, respectively). As the bead moved away from the centre of the trap due to CENP-E motor activity, it experienced greater trapping force and eventually detached and snapped back to the centre of the trap (Movie S4). These repeated motions led to the characteristic displacement spikes recorded with a quadrant photodetector (Fig. 2C). While the force values generated by CENP-E on D-MTs extended into the 8 pN range, such large forces were infrequent on T-MTs (Fig. 2C, Fig. S9C). Consistently, the average duration of the force spikes was longer on D-MTs vs. T-MTs (0.79±0.05 vs. 0.49±0.02 s, Fig. S9D). Thus, CENP-E is unable to sustain large loads on T-MTs, in line with the persistence of pole-proximal chromosomes after inhibition of microtubule detyrosination in spindles (Fig. 1B).

To investigate the CENP-E stepping mechanism on different microtubule lattices we analysed high-resolution bead recordings (Fig. 2D,E). On both types of microtubules, the average step size was ~8 nm (Fig. S9E), as expected based on tubulin dimer spacing in the microtubule lattice (24). Backward steps were frequently observed and, with increasing trap load, the probability of a forward step decreased more gradually for CENP-E (Fig. 2F, Fig.

S9F), than for Kinesin-1 (25, 26). Although the forward stepping of CENP-E was slightly more frequent on D-MTs vs. T-MTs, the overall dependency of CENP-E stepping on the resisting force was similar on these two lattices. The average dwell time between the steps for the entire force range was also similar on D- and T-MTs (Fig. S9G). We further observed a slightly shorter dwell time at low force on D-MTs, which is consistent with the faster velocity of CENP-E walking on this type of microtubules (Fig. 2G). Importantly, CENP-E responded to larger loads by prolonging its dwells on D-MTs, but not on T-MTs. Under the load, CENP-E also detached less frequently from D-MTs (Fig. 2H). As a result, the peak force for CENP-E detachment was shifted to significantly higher values on D-MTs (Fig. 2I), indicating that the effect of tubulin detyrosination is exerted mostly on CENP-E detachment, rather than stepping. Thus, CENP-E can carry a significantly larger load on D-MTs in vitro.

Our data support a model in which CENP-E-dependent transport of pole-proximal chromosomes towards the spindle equator requires microtubule tracks that are detyrosinated. Therefore, increasing tubulin detyrosination should disrupt the biased motion of pole-proximal chromosomes towards the equator and cause their delivery to inappropriate cellular locations. To test this, we increased tubulin detyrosination by depleting TTL by RNAi in U2OS cells (Fig. S10A). Immunofluorescence analysis confirmed that TTL depletion caused ubiquitous detyrosination of spindle microtubules (including astral microtubules) during early mitosis (Fig. S10B and ref. (27)). Live-cell imaging revealed that 65% of TTL-depleted cells delayed mitotic progression and failed to congress all the chromosomes (Fig. 3A, Movie S5). In these cells, the pole-proximal chromosomes did not remain stuck at the spindle poles, as observed after CENP-E inhibition or after blocking tubulin detyrosination, but were transported in various directions, including towards the cell cortex (Fig. 3A,B). This suggests that the spatial cues that normally guide CENP-E towards the equator were disrupted. CENP-E inhibition in live TTL-depleted cells significantly decreased the transport of chromosomes away from spindle poles (Fig. 3A,B). This was confirmed in a large population of fixed cells using a quantitative monopolar spindle configuration assay (1) (Fig. 4A–C), indicating that the random transport of chromosomes along ubiquitously detyrosinated spindle microtubules after TTL RNAi is mediated by CENP-E.

Taken together, our work establishes the specific molecular mechanism that guides CENP-E-dependent chromosome motion towards the cell equator. This mechanism is based on the ability of CENP-E to transport pole-proximal chromosomes preferentially on detyrosinated microtubule tracks, which are normally oriented towards the spindle equator (Fig. S11). We propose that microtubule detyrosination, as part of the “tubulin code”, works as a navigation system that guides kinetochore motors during cell division, ultimately contributing to faithful chromosome segregation.

Supplementary Material

Refer to Web version on PubMed Central for supplementary material.

Acknowledgments

We thank F.I. Ataullakhanov for help with the laser trap and data analysis, A. Kiyatkin, V. Mustyatsa, M. Molodtsov, A. Gautreau, G. Lakisic and Martina Barisic for technical assistance, and members of our laboratories for stimulating discussions. This work was supported by National Institutes of Health Grant R01-GM098389 and RSG-14-018-01-CCG from the American Cancer Society to ELG; by the Institut Curie, the CNRS, the INSERM, the ANR award ANR-12-BSV2-0007, INCA_6517, ANR-10-LBX-0038 part of the IDEX Idex PSL ANR-10-IDEX-0001-02 PSL to CJ; FLAD Life Science 2020 and PRECISE grant from the European Research Council to HM. AVZ is supported by the Russian Academy of Sciences Presidium Grants “Mechanisms of the Molecular Systems Integration”, “Molecular and Cell Biology programs” and Russian Fund for Basic Research Grant 12-04-00111-a and 13-00-40188. RSS is supported by a fellowship from the GABBA PhD program from the University of Porto. ALP is supported by fellowship SFRH/BPD/66707/2009 from Fundação para a Ciência e a Tecnologia of Portugal. MB, RSS, SKT, MMM, CJ, ELG, HM - designed experiments; MB – performed all experiments in cells; MMM - established and performed the tubulin purification protocol from HeLa cells; RSS - performed single molecule experiments; SKT - performed force measurements; ALP - provided reagents; all authors analysed data; HM, ELG, MB - wrote the paper, with contributions from all authors; HM – conceived and coordinated the project. Data described can be found in the main figures and supplementary materials.

References and Notes

1. Barisic M, Aguiar P, Geley S, Maiato H. Kinetochore motors drive congression of peripheral polar chromosomes by overcoming random arm-ejection forces. Nature cell biology. 2014; 16
2. Kapoor TM, et al. Chromosomes can congress to the metaphase plate before biorientation. Science. 2006; 311:388–391. [PubMed: 16424343]
3. Walczak CE, Cai S, Khodjakov A. Mechanisms of chromosome behaviour during mitosis. Nat Rev Mol Cell Biol. 2010; 11:91–102. [PubMed: 20068571]
4. Kalab P, Heald R. The RanGTP gradient - a GPS for the mitotic spindle. Journal of cell science. 2008; 121:1577–1586. [PubMed: 18469014]
5. Kiyomitsu T, Cheeseman IM. Chromosome- and spindle-pole-derived signals generate an intrinsic code for spindle position and orientation. Nat Cell Biol. 2012; 14:311–317. [PubMed: 22327364]
6. Kim Y, Holland AJ, Lan W, Cleveland DW. Aurora kinases and protein phosphatase 1 mediate chromosome congression through regulation of CENP-E. Cell. 2010; 142:444–455. [PubMed: 20691903]
7. Whyte J, et al. Phosphorylation regulates targeting of cytoplasmic dynein to kinetochores during mitosis. The Journal of cell biology. 2008; 183:819–834. [PubMed: 19029334]
8. Cai S, O'Connell CB, Khodjakov A, Walczak CE. Chromosome congression in the absence of kinetochore fibres. Nature cell biology. 2009; 11:832–838. [PubMed: 19525938]
9. Verhey KJ, Gaertig J. The tubulin code. Cell Cycle. 2007; 6:2152–2160. [PubMed: 17786050]
10. Janke C. The tubulin code: molecular components, readout mechanisms, and functions. J Cell Biol. 2014; 206:461–472. [PubMed: 25135932]
11. Gundersen GG, Bulinski JC. Distribution of tyrosinated and nontyrosinated alpha-tubulin during mitosis. The Journal of cell biology. 1986; 102:1118–1126. [PubMed: 3512580]
12. Wilson PJ, Forer A. Acetylated α-tubulin in spermatogenic cells of the crane fly Nephrotoma suturalis: Kinetochore microtubules are selectively acetylated. Cell Motil. Cytoskeleton. 1989; 14:237–250.
13. Gundersen GG, Kalnoski MH, Bulinski JC. Distinct populations of microtubules: tyrosinated and nontyrosinated alpha tubulin are distributed differently in vivo. Cell. 1984; 38:779–789. [PubMed: 6386177]
14. Reed NA, et al. Microtubule acetylation promotes kinesin-1 binding and transport. Curr Biol. 2006; 16:2166–2172. [PubMed: 17084703]
15. Konishi Y, Setou M. Tubulin tyrosination navigates the kinesin-1 motor domain to axons. Nat Neurosci. 2009; 12:559–567. [PubMed: 19377471]
16. Hammond JW, et al. Posttranslational modifications of tubulin and the polarized transport of kinesin-1 in neurons. Molecular biology of the cell. 2010; 21:572–583. [PubMed: 20032309]
17. Sirajuddin M, Rice LM, Vale RD. Regulation of microtubule motors by tubulin isotypes and post-translational modifications. Nat Cell Biol. 2014; 16:335–344. [PubMed: 24633327]

18. Ersfeld K, et al. Characterization of the tubulin-tyrosine ligase. The Journal of cell biology. 1993; 120:725–732. [PubMed: 8093886]
19. Fonrose X, et al. Parthenolide inhibits tubulin carboxypeptidase activity. Cancer Res. 2007; 67:3371–3378. [PubMed: 17409447]
20. Poser I, et al. BAC TransgeneOmics: a high-throughput method for exploration of protein function in mammals. Nat Methods. 2008; 5:409–415. [PubMed: 18391959]
21. Yen TJ, Li G, Schaar BT, Szilak I, Cleveland DW. CENP-E is a putative kinetochore motor that accumulates just before mitosis. Nature. 1992; 359:536–539. [PubMed: 1406971]
22. Please see Supplementary Materials for details.
23. Gudimchuk N, et al. Kinetochore kinesin CENP-E is a processive bi-directional tracker of dynamic microtubule tips. Nat Cell Biol. 2013; 15:1079–1088. [PubMed: 23955301]
24. Yardimci H, van Duffelen M, Mao Y, Rosenfeld SS, Selvin PR. The mitotic kinesin CENP-E is a processive transport motor. Proc Natl Acad Sci U S A. 2008; 105:6016–6021. [PubMed: 18427114]
25. Carter NJ, Cross RA. Mechanics of the kinesin step. Nature. 2005; 435:308–312. [PubMed: 15902249]
26. Nishiyama M, Higuchi H, Yanagida T. Chemomechanical coupling of the forward and backward steps of single kinesin molecules. Nat Cell Biol. 2002; 4:790–797. [PubMed: 12360289]
27. Peris L, et al. Tubulin tyrosination is a major factor affecting the recruitment of CAP-Gly proteins at microtubule plus ends. J Cell Biol. 2006; 174:839–849. [PubMed: 16954346]

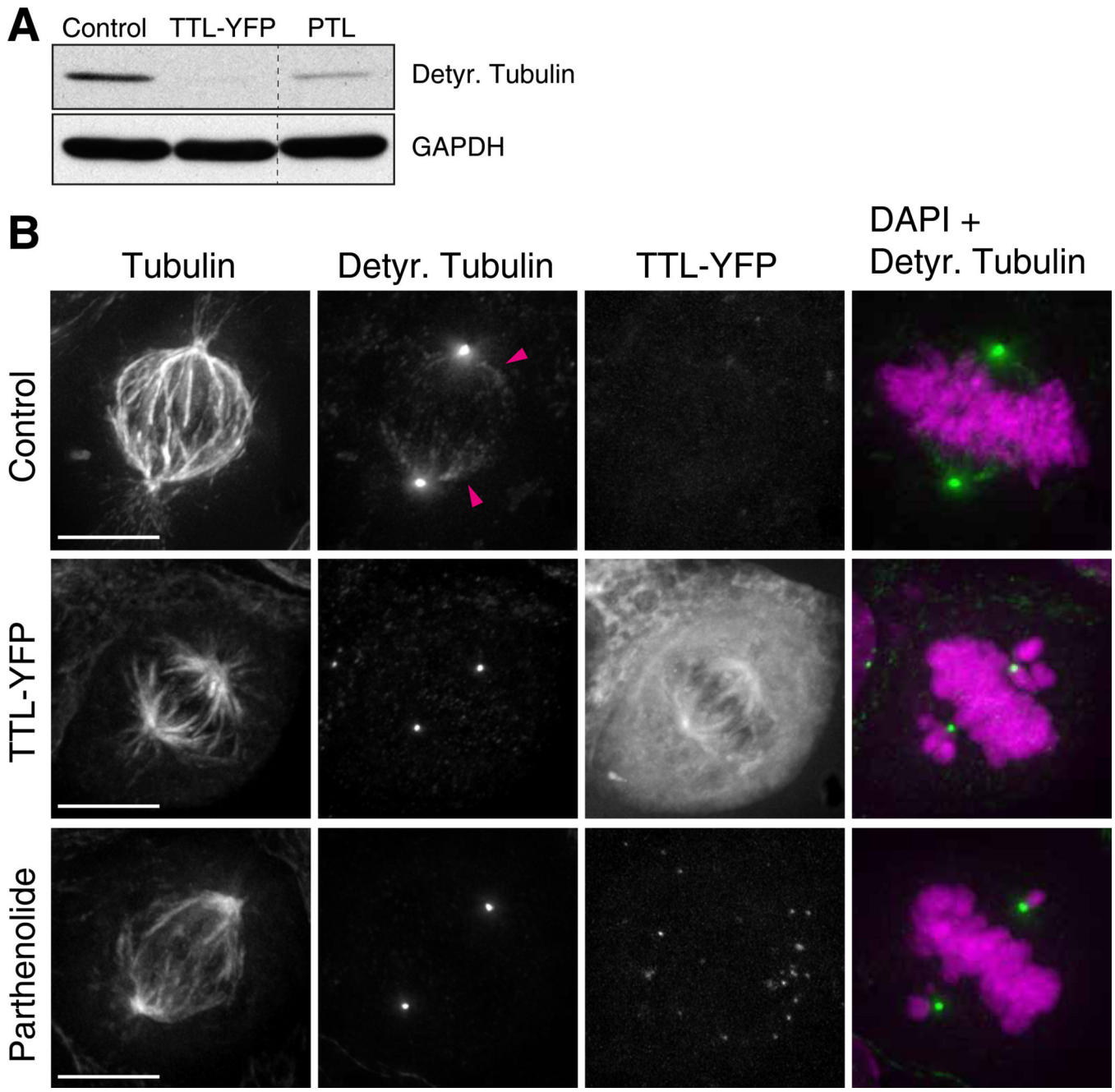

Fig. 1. Chromosome congression requires spatially regulated detyrosination of spindle microtubules

(**A**) Microtubule detyrosination was examined by immunoblotting with detyrosinated tubulin antibodies. Protein lysates of U2OS cells were obtained 24h after TTL-YFP transfection and 4h after adding parthenolide (20 μM). GAPDH was used as loading control. (**D**) Deconvolved immunofluorescence images of U2OS cells stained for DNA (DAPI=magenta), α-tubulin and detyrosinated tubulin (green). TTL-YFP signal was detected by direct fluorescence. Arrowheads highlight detyrosinated spindle microtubules in

control cells. Detyrosination of spindle microtubules is undetectable after TTL-YFP over-expression or treatment with parthenolide. Scale bar = 10 μm.

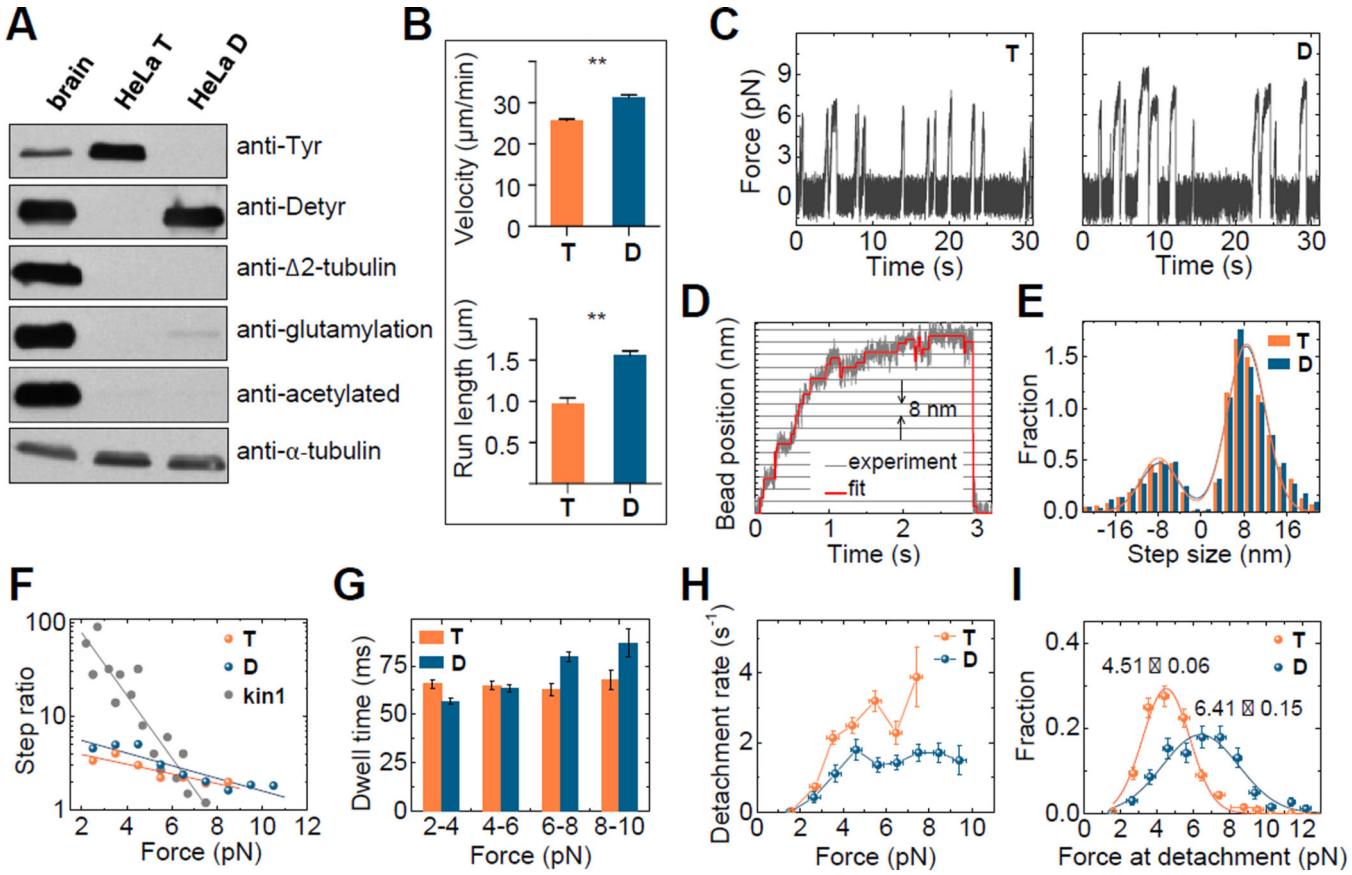

Fig. 2. CENP-E motility is enhanced on detyrosinated microtubules in vitro

(**A**) Immunoblot of purified tubulin from porcine brain or HeLa cells before (T) and after (D) detyrosination with carboxypeptidase A. Antibodies against tyrosinated, detyrosinated, Δ2, glutamylated (GT335) and acetylated tubulin were used to assess post-translational modifications. Anti-α-tubulin antibody demonstrates similar amounts of tubulin in different lanes. (**B**) Mean velocity and characteristic run length of CENP-E for D-MTs (N=4 independent experiments, n=401) and T-MTs (N=3, n=257 molecules). Error bars are SEMs; **p≤0.01 based on unpaired t-test with 95% confidence. (**C**) Typical traces of bead motions on D- and T-MTs, plotted as force vs. time. **(D)** Example trace of CENP-E bead in a laser trap with step-size fit. (**E**) Step size histograms were fit by the sum of two Gaussians (lines). Positive steps were away from the trap's centre. Number of forward steps was 3427 and 5146; backward steps 1114 and 1731 for D- and T-MTs, respectively. (**F**) Ratio of forward to backward steps for CENP-E in comparison to Kinesin-1 (data from (25, 26)) with theoretical fittings for ratio >1. (**G**) Characteristic dwell times as a function of force within 2 pN bins. Total number of dwells for all forces was 4541 and 6877 for D- and T-MTs, respectively. (**H**) CENP-E detachment rate under load. Error bars for detachment rate were calculated by dividing the square root of the number of detachments by the total time within each bin. Error bars for force are SEM for measurements in each bin. (**I**) Histograms of detachment force with Gaussian fits. Numbers are the Mean±SEM, n=269 for D-MTs, and 491 for T-MTs. Vertical error bars are square roots of the number of detachments normalized by the total number of detachments.

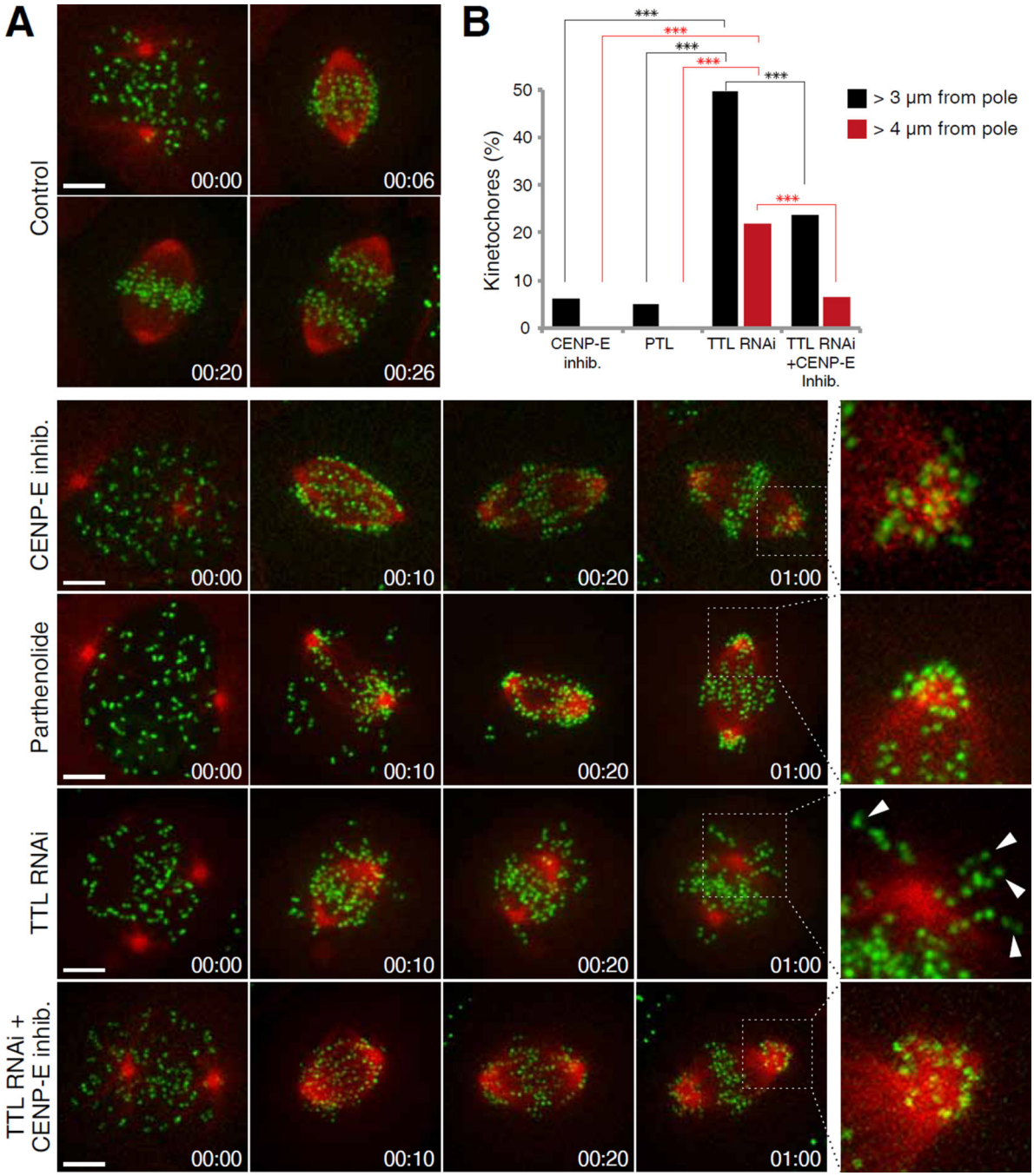

Fig. 3. Chromosomes cannot complete congression in TTL depleted cells and are randomly transported away from the spindle pole by CENP-E

(**A**) Spinning-disk confocal imaging of live U2OS cells stably expressing CENP-A-GFP and mCherry-tubulin. Chromosome congression was impaired in 100% of cells treated either with CENP-E inhibitor (13 cells, 3 independent experiments) or parthenolide (9 cells, 2 independent experiments). Chromosome congression was impaired in 65% of cells depleted of TTL (23 cells, 3 independent experiments). Arrowheads highlight kinetochores transported away from the spindle pole towards the cell cortex. Enlarged insets highlight

polar regions. Scale bar = 5 μm. Time = h:min. (**B**) Quantification of the percentage of pole-proximal chromosomes that were transported away from spindle poles in the different conditions. N(CENP-E inh.)=311 kinetochores from 10 cells, 3 independent experiments; N(parthenolide)=388 kinetochores from 7 cells, 2 independent experiments; N(TTL RNAi)=311 kinetochores from 18 cells, 3 independent experiments. N(TTL RNAi+CENP-E inh)=720 kinetochores from 17 cells, 3 independent experiments. Asterisks indicate z test significance values;***p<0.001.

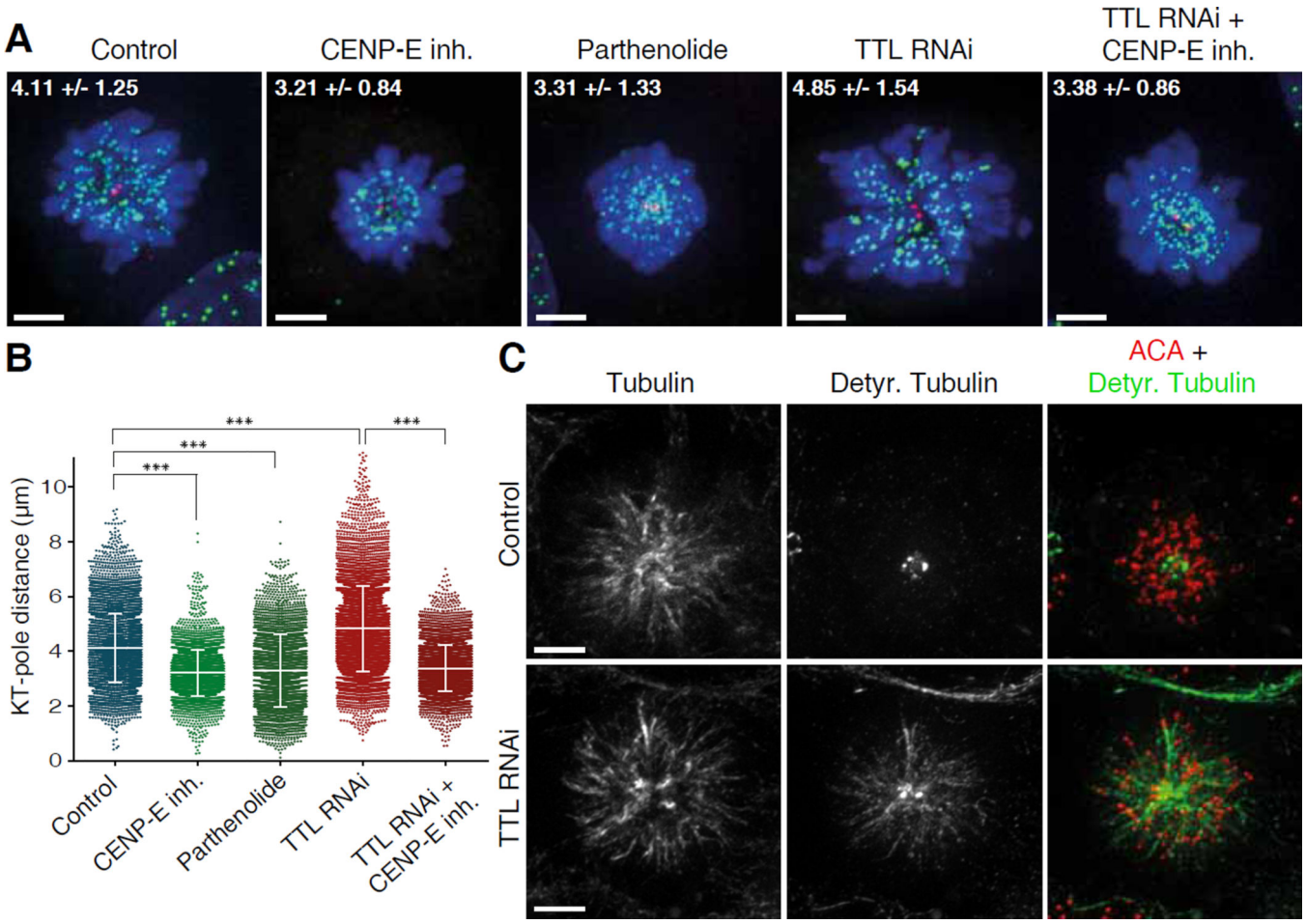

Fig. 4. CENP-E-dependent transport of pole-proximal chromosomes along ubiquitously detyrosinated spindle microtubules after TTL RNAi

(**A**) U2OS cells treated with the kinesin-5 inhibitor S-Trytil-L-Cysteine (STLC) and immunostained for DNA (DAPI=blue), kinetochores (ACA=green) and centrioles (centrin=red). Maximum intensity projection images of representative examples for each condition are shown. Numbers indicate mean kinetochore-to-pole distances ± SD of the pooled data from at least two independent experiments per condition. Scale bar = 5 µm. (**B**) Quantification of kinetochore (KT) to pole distances in STLC-treated cells under different conditions; n(Control)=7185 kinetochores from 56 cells, 3 experiments; n(CENP-E inh)=3877 kinetochores from 34 cells, 2 experiments; n(Parthenolide)=3611 kinetochores from 30 cells, 2 experiments; n(TTL RNAi)=8239 kinetochores from 61 cells, 4 experiments; n(TTL RNAi + CENP-E inh)=5458 kinetochores from 45 cells, 2 experiments. Asterisks indicate Mann-Whitney U-Test significance values: ***p<0.001. (**C**) Deconvolved immunofluorescence images of STLC-treated U2OS cells stained for α-tubulin, detyrosinated tubulin and ACA. Detyrosination of spindle microtubules was highly increased after TTL RNAi. Scale bar = 5 µm.